Available online at www.sciencedirect.com

ScienceDirect

Procedia Engineering 00 (2016) 000–000

Procedia Engineering

www.elsevier.com/locate/procedia

1st International Conference on the Material Point Method, MPM 2017

Analysis of crater development around damaged pipelines using the material point method

Mario Martinelli[a,*], Faraz S. Tehrani[a], Vahid Galavi[a]

[a]*Deltares, Delft, The Netherlands*

Abstract

In this study, the material point method (MPM) is used to simulate and analyze crater development around a pipeline embedded in sand. To that end, a *double-point* MPM formulation in conjunction with an elastic-perfectly plastic soil model with Mohr-Coulomb failure criterion is used to simulate the onset and evolution of crater in fully saturated sands. The onset of failure is also simulated with standard finite element method. The results show that the *double-point* MPM formulation can satisfactorily capture the essential features of the crater development.

Peer-review under responsibility of the organizing committee of the 1 st International Conference on the Material Point Method.

Keywords: material point method, crater, pipeline, failure, fluidisation.

1. Introduction

When a water pipeline is damaged, it is very likely that a crater is developed around the damaged area. This can impose a high risk to urban environment where a network of underground pipelines is present. Therefore, it is highly important to understand the mechanism of crater development around damaged pipelines to minimize the risk associated with this phenomenon and to provide practical recommendations to prevent catastrophic consequences of pipeline damage.

Crater development around a damaged buried pipeline is a soil-fluid interaction problem which includes large deformation of soil around the damaged area. Therefore, simulation of the entire process cannot be carried out using

* Corresponding author.
E-mail address: mario.martinelli@deltares.nl

Peer-review under responsibility of the organizing committee of the 1 st International Conference on the Material Point Method.

small-deformation analysis methods. Hence, use of a large deformation analysis approach such as the Material Point Method (MPM) that can take into account the interaction of soil and water is rather appealing.
The original formulation of MPM was developed by Harlow (1964) [1] for fluid mechanics and then applied to solid mechanics [2] and dry granular materials [3-5]. Later, the method was extended to handle saturated soils [6] with a numerical approach which uses the velocity of both solid and liquid constituent as the primary unknowns. This formulation was applied to several small and large deformation problems and is able to capture the physical response of saturated soil under dynamic loading. However, only one set of material points is used for both the solid and the liquid phase; therefore groundwater flow and the transition between free water and groundwater cannot be captured as well as fluid-like behaviour of the soil, which is typical in fluidisation and sedimentation problems. Recently, a formulation with two sets of material points (so called *double-point* formulation) was proposed [7-10] to overcome such limitations. Refinements to the original *double-point* formulation were first presented in [11] and then extended in [12], which is finally used in the current study.

2. Concepts of the *double-point* MPM

The motion of both water and solid material points (MP) is described by the system of momentum balance equations, using separate velocity fields $\boldsymbol{v}_S$ and $\boldsymbol{v}_L$ for solid and liquid constituents, respectively:

$$\nabla \cdot \boldsymbol{\sigma}'_S + (1-n)\nabla \cdot \boldsymbol{\sigma}_L + \bar{\rho}_S \boldsymbol{g} + \boldsymbol{f}_d = \bar{\rho}_S \frac{D^S \boldsymbol{v}_S}{Dt} \tag{1}$$

$$n(\nabla \cdot \boldsymbol{\sigma}_L) + \bar{\rho}_L \boldsymbol{g} - \boldsymbol{f}_d = \bar{\rho}_L \frac{D^L \boldsymbol{v}_L}{Dt} \tag{2}$$

where $\bar{\rho}_S$ and $\bar{\rho}_L$ represent respectively the partial densities of the solid and liquid, which is the ratio of the mass of each constituent with respect to the reference volume; n is the soil porosity; $\boldsymbol{\sigma}'_S$ is the effective stress tensor for solid; $\boldsymbol{\sigma}_L$ is the stress tensor for liquid; and $\boldsymbol{g}$ is the gravity vector. In equations (1)and(2), $\boldsymbol{f}_d$ is the drag force vector exerted by the liquid on the solid part. The drag force includes the non-linear velocity term that describes the additional drop of the hydraulic head observed at high flow velocities, which is common in soils with large porosity. The Forchheimer [13] equation is used to compute $\boldsymbol{f}_d$ as:

$$\boldsymbol{f}_d = n^2 \frac{\mu}{\kappa}(\boldsymbol{v}_L - \boldsymbol{v}_S) + \frac{F}{\sqrt{\kappa}} n^3 \rho_L \,|\boldsymbol{v}_L - \boldsymbol{v}_S|\,(\boldsymbol{v}_L - \boldsymbol{v}_S) \tag{3}$$

where μ is the dynamic viscosity of liquid and κ is the soil intrinsic permeability. The Kozeny-Carman formula [14] is used to update the soil intrinsic permeability as follows,

$$\kappa = \frac{D_p^2}{A} \frac{n^3}{(1-n)^2} \tag{4}$$

where D_p is the average grain size diameter and the coefficients F is computed as:

$$F = \frac{B}{\sqrt{A} n^{3/2}} \tag{5}$$

where B is a constant set to 1.75 [15]. A is also a constant which is equal to 150 according to Ergun [15].

This formulation can distinguish between mixtures characterized by low and high porosities (see Fig. 1). Fig. 1(a) shows a low-porosity mixture, where the grains of the solid skeleton are in close contact and the behaviour can be described by constitutive models developed for granular materials (solid-like response). Conversely, as shown in Fig. 1(b), in a high-porosity mixture the grains are not in contact and float together with the liquid phase. In this case, the effective stresses are equal to zero and the response of the mixture is described by the Navier-Stokes equation (liquid-like response).

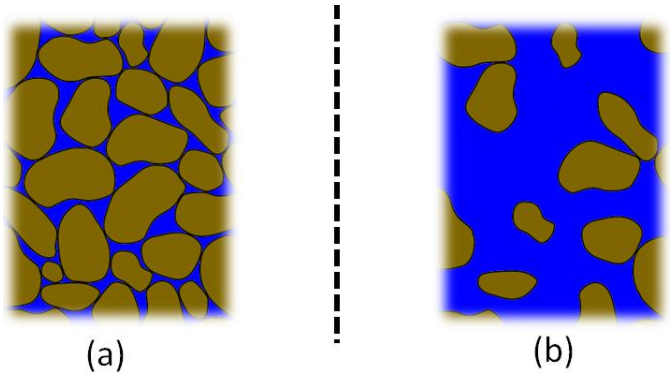

Fig. 1. Solid-liquid mixture with (a) low porosity and (b) high porosity.

In the current formulation, the two aforementioned states are distinguished through the maximum porosity n_{max}, which is the maximum value of the porosity for a given soil in its loosest state (corresponding to e_{max}). During the fluidization process, when the mixture porosity is lower than the maximum porosity ($n<n_{max}$), the decrease in the mean effective stress results in increase in the porosity. When the contact forces between the grains vanish, the mean effective stress becomes nil. However, the fluidisation occurs only if the grains are significantly separated, so that the porosity is larger than n_{max}. In the reverse process, i.e. the sedimentation of a fluidized mixture, the porosity decreases due to the fact that the solid grains get closer to each other. However, the effective stresses recur only if the porosity is smaller than n_{max}, i.e. the grains are close enough to be in contact.

In case of *solid-like* response, the effective stress rate in solid MPs is calculated using the constitutive law. In case of *liquid-like* response, the effective stress in solid MPs is set to zero. Equation (2) is used to describe the behavior of water in the soil-water mixture. The pore pressure is computed using the volumetric strain and the water bulk modulus. Conversely, the deviatoric stress tensor is computed using the liquid strain rate tensor and a viscosity which takes into account the solid concentration ratio of the mixture. In case of solid-like behavior the deviatoric stress tensor is set to zero.

3. Crater development around a damaged pipeline in sand

The *double-point* MPM is used to model the crater development induced by discharge of a damaged pipeline. A pipeline with diameter of 1.15 m is embedded 2.5 m below the ground level in a homogeneous and saturated sand layer. The geometry of the problem is shown in Fig. 2 where only one quarter of the pipeline cross section is presented. In the MPM simulation, the pipe is replaced by an equivalent square with 1 m long sides. The pipeline is damaged in crown within -45 and +45 degrees around the vertical axis, and in the equivalent square cross section this damage is on the top side of the square. The pipe is full of water and the hydraulic head is assumed to be 12 m at the beginning of the simulation.

A linear elastic perfectly plastic constitutive model with a Mohr-Coulomb failure criterion is used for the solid skeleton and a Newtonian compressible constitutive model is used for the liquid phase. The parameters for both constitutive models are listed in Table 1.

Table 1. Parameters of the constitutive models of water.

Material parameter	*Symbol*	*Value*	*Unit*
Water density	ρ_L	1000	kg/m^3
Water bulk modulus	K_L	50000	kPa
Water viscosity	μ	8.905 10^{-7}	kPa.s

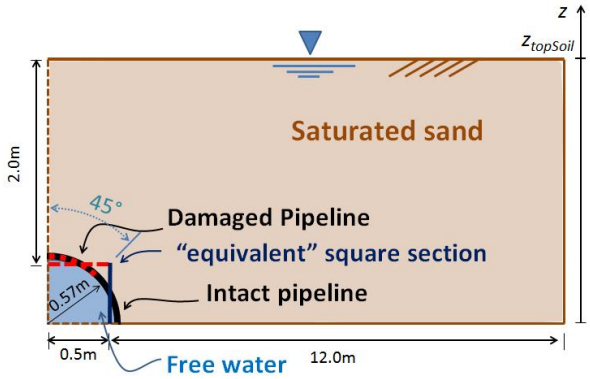

Fig. 2. Geometry of the problem.

Table 2. Parameters of the constitutive models of soils.

Material parameter	*Symbol*	*Value*		*Unit*
		Loose sand	*Dense sand*	
Density of soil grains	ρ_S	2700	2700	kg/m^3
Young modulus of soil	E	1000	10000	kPa
Poisson ratio of soil	ν	0.2	0.2	-
Initial porosity	n	0.45	0.4	-
Maximum porosity	n_{max}	0.5	0.5	-
Solid grain diameter	D_p	2	2	mm
Friction angle	φ	30	35	degree
Dilatancy angle	ψ	0	0	degree
Cohesion	c	1	10	kPa

Plane-strain conditions are assumed in the simulation. The computational mesh shown in Fig. 3 consists of 29064 4-node tetrahedral elements. The water in the pipe is supplied by a reservoir, large enough to approximately maintain the initial water level throughout the simulation. At the beginning of the calculation, 8 material points (MPs) per element (4 liquid and 4 solid MPs) are assigned to the soil domain and 4 MPs are assigned to the free water. At all boundaries, including the pipeline, the displacements are constrained in normal direction and free in the longitudinal direction. The damage in the pipeline is simulated by removing the fixities of the water displacements.

The initial stress in the water is hydrostatic. The effective stress in the solid skeleton is set to:

$$\sigma'_{S,zz} = (\bar{\rho}_S - \rho_L) g (z - z_{topSoil})$$
$$\sigma'_{S,xx(t=0)} = \sigma'_{S,yy(t=0)} = K_0 \sigma'_{S,zz} \quad (6)$$

where $z_{topSoil}$ is the value of the vertical axis at the top of the saturated sand (see Fig. 2) and K_0 is the coefficient of lateral earth pressure assumed to be equal to 0.5. Since Equations (1) and (2) are solved with an explicit time integration scheme, the bulk modulus of the water is reduced by a factor of 20 in order to reduce the computational time but still large enough compared to the bulk modulus of the solid skeleton.

Two cases are considered in the simulations: loose and dense sand. The loose sand is characterized by an initial porosity of 0.45, Young's modulus of 1 MPa, cohesion of 1 kPa and friction angle of 30 degrees whereas, for the dense sand the initial soil porosity is 0.4, the Young's modulus is 10 MPa, the cohesion is 10 kPa and the friction angle is 35 degrees.

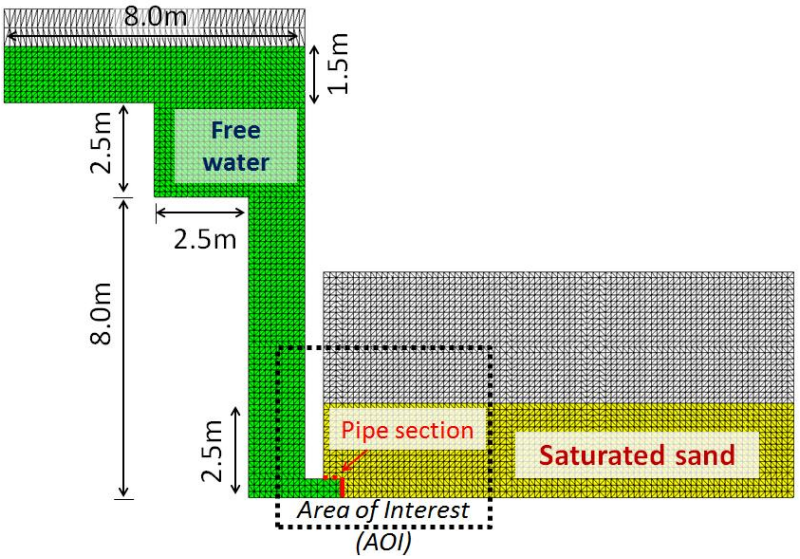

Fig. 3. Discretised domain of the simulated problem.

The soil permeability is calculated according to Kozeny-Carman formula [14] using the updated porosity, resulting in k = 5.3 cm/s and 8.8 cm/s (respectively for dense and loose sand) at the beginning of the simulation. The results are shown only over a limited part of the domain labeled as “area of interest” (AOI) as shown in Fig. 3.

3.1. Dense sand

Fig. 4 shows the soil porosity at the location of the solid material points for t = 2, 3, 4, 5 and 6 seconds, together with the position of the liquid material points. The porosity can vary approximately from 0.4 to 1.0 but the legend has a narrower limit to focus on the range of solid-like behaviour (n < 0.52).

As soon as a horizontal “crack” is generated, the liquid vertical fixities are deactivated, and the water in the pipeline starts flowing upward into the saturated soil. Due to the large difference in the hydraulic head that exists between the free water and the ground water, large drag forces are exerted to the solid grains. The soil in contact with the pipe moves upward and the porosity of the soil close to the pipe increases (t=2s).

As the time passes (t=3s), an inclined wedge-shape failure surface is generated into the soil. The porosity along the failure surface increases until it exceeds the maximum porosity when the soil fluidizes. Fluidized material is also observed at the ground surface, close to the left boundary. This is the result of the finite clockwise rotation of the soil wedge which locally increases the soil porosity.

As the calculation progresses (t=4s-6s), the extension of the fluidized zone progressively increases until the failure wedge is completely fluidized and is consequently pushed away by the water flow along the ground level.

3.2. Loose sand

The results for the loose sand are shown in Fig. 5 for t=0.4, 0.8 and 1.6s. The failure mechanism is quite different than for the dense sand. The soil moves upward very rapidly, sliding along a sub-vertical failure surface (t=0.4-0.8). The fluidization process is very fast, so that after 1.6s the entire soil above the pipe crack is completely fluidized. Moreover, since the water flow is significantly high, the soil along the failure surface is dragged away by the flow and the thickness of the fluidized soil progressively increases towards the right side of the domain.

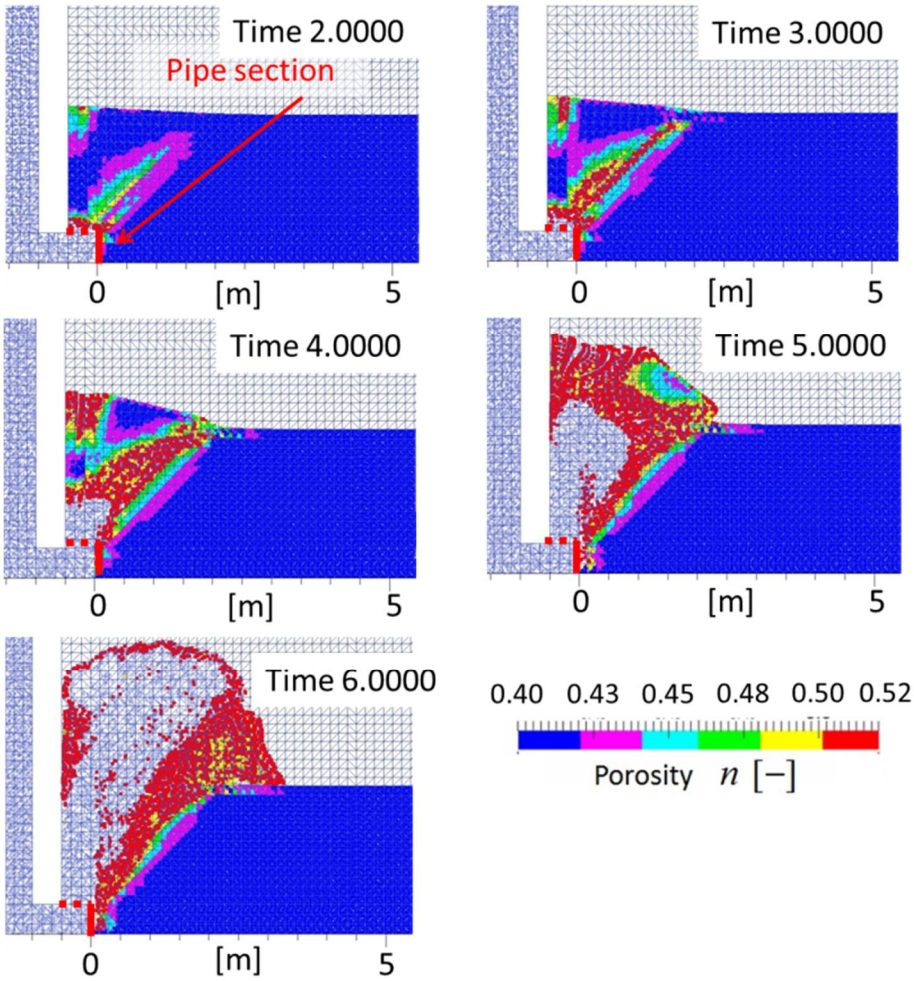

Fig. 4. Porosity of solid material points in the dense sand problem.

3.3. Modeling the onset of failure with FEM

The problem is also simulated using standard (small-deformation) FEM with the commercial code PLAXIS 2D [16], where the onset of failure is simulated under undrained and drained condition with the small strain FE formulation.

The geometry and the soil parameters are the same as those used in the MPM simulations. The mesh is composed of 1964 15-node triangular elements. Since the water velocity is very high compared to the seepage flow, the water pressure in the pipe is modeled as an external load of 115 kPa (11.5 m of water) acting directly on the soil (in upward direction).

The analysis type is set to “plastic” and no seepage flow is considered. The inertia terms are also neglected. However, the excess pore pressures are computed in case of undrained conditions. It should be noted that although the rate of loading is high and consequently the hydrodynamic period is low, as a simplifying assumption in FE analyses, an undrained quasi-static approach is used to describe the onset of failure. Using such simplifying assumption it is observed that for certain values of external loads no equilibrium can be reached.

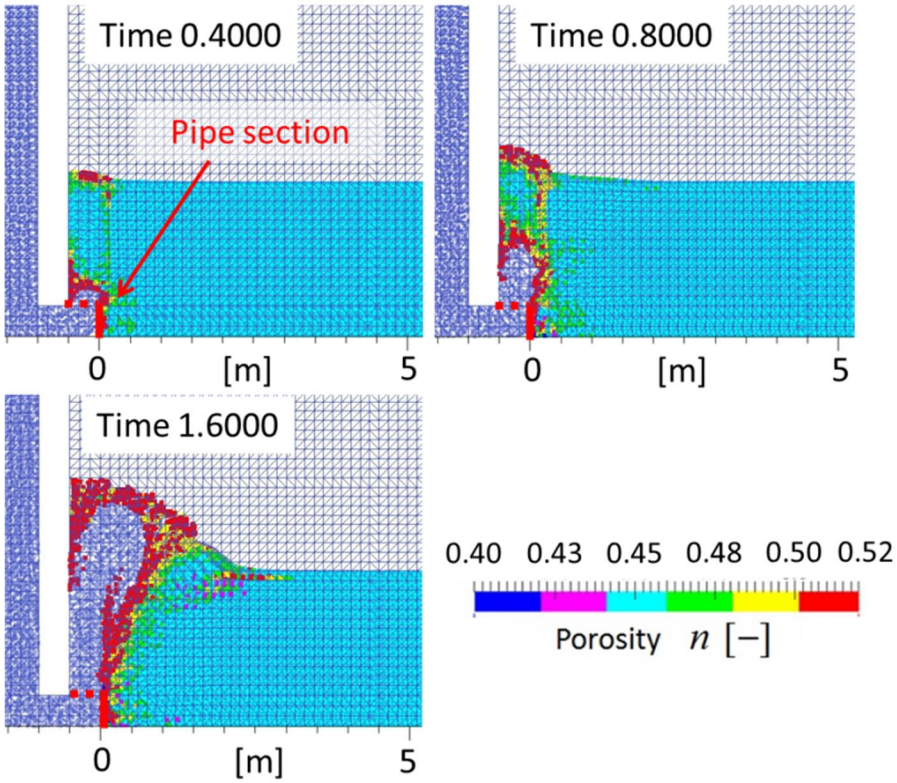

Fig. 5. Porosity of solid material points in the loose sand problem.

The vertical displacements contour is plotted in Fig. 6 for each soil type and analysis condition, at the last step the calculation converges. The contours describe more or less the same phenomena observed from the MPM analyses. In the dense sand deposit, the failure surface next to the pipe section is inclined with respect to the horizontal axis, with an angle of approximately 45 degrees in drained condition and 60 degrees in undrained one. Conversely, for loose sand deposit, the vertical displacement is mostly concentrated in the soil directly above the pipe which implies the localization of failure in the loose sand

It is worth mentioning that this analysis cannot provide any additional information regarding the evolution of crater. Such information can only be obtained when performing not only dynamic coupled flow-deformation analyses but also taking into account large deformations by updating the mesh (Updated-Lagrangian formulation). However, in this case, even the large deformation approach suffers from element distortion and cannot be used to properly capture the evolution of the crater; therefore MPM is a suitable approach for this purpose, because it can simulate the problem from the beginning, where the displacements are small, towards the end after extremely large deformation.

4. Conclusions

Onset and progression of crater around a damaged pipeline were simulated in this study using the *double-point* MPM for a loose and dense soil deposit. It was shown that the MPM can satisfactorily simulate the problem. Furthermore, the onset of failure during carter development was simulated using the FEM to verify the MPM results. However, the FEM analysis could not provide any additional information regarding the evolution of the crater. Even large deformation FE approach suffers from element distortion and cannot be used to properly capture the evolution or the crater.

Lastly, it is worth mentioning that the differences between the behavior of loose and dense sand not only involve differences in porosity and strength, but it also depends on the constitutive behavior, i.e. contracting and dilatant response. This aspect will be investigated in future studies.

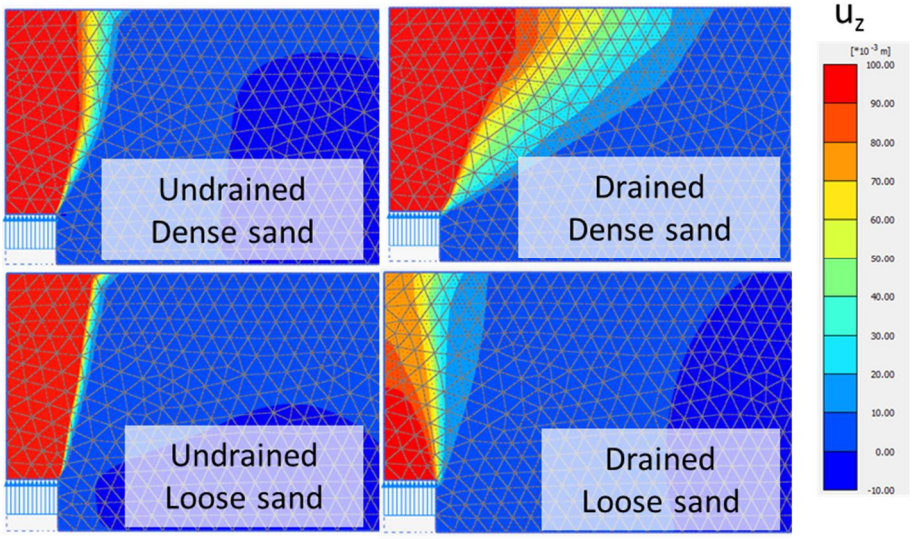

Fig. 6. Vertical displacements obtained from FE simulations at the last step at which the calculation converges.

References

[1] Harlow F.H. The particle-in-cell computing method in fluid dynamics. *Methods in Computational Physics*. 1964; 3, pp 319-343.
[2] Sulsky D., Zhou S., Schreyer H.L. Application of a particle-in-cell method to solid mechanics. *Computer Physics Communications*. 1995 ,87, pp 236-252.
[3] Wieckowski Z. A particle-in-cell method in analysis of motion of a granular material in a silo. In: *Computational Mechanics: New Trends and Applications*, CIMNE, Barcelona, 1998
[4] Wieckowski Z., Youn S.K., Yeon Y.H. A particle-in-cell solution to the silo discharging problem. *Int. J. Numer. Meth. Engng*, 1999, 45, pp 1203-1225.
[5] Wieckowski Z. Modelling of silo discharge and filling problems by the material point method. *Task Quarterly*, 2003, 4, pp 701-721.
[6] Jassim I., Stolle D., Vermeer P.A. Two-phase dynamic analysis by material point method. *International Journal for Numerical and Analytical Methods in Geomechanics 37(15), 2502-2522*; 2013, DOI:10.1002/nag.2146
[7] Bandara S., Soga K. Coupling of soil deformation and pore fluid flow using material point method. *Computers and Geotechnics*; 2015, 63, 199-214. DOI:10.1016/j.compgeo.2014.09.009.
[8] Bandara S. Material Point Method to simulate large deformation problems in fluid-saturated granular medium. *Ph.D. Thesis* University of Cambridge, 2013.
[9] Vermeer P.A., Wieckowski Z., Sittoni L., Beuth L. Modelling Soil-Fluid and Fluid-Soil Transitions with Applications to Tailings. In: *Tailings and Mine Waste*, November 3-6, 2013, Ban, Alberta, Canada, pp. 305-315.
[10] Więckowski Z. *Enhancement of the Material Point Method for Fluid-Structure Interaction and Erosion*. Report on EU-FP7 research project Geo Fluid PIEF-GA-2010-274335, 2013.
[11] Martinelli M. and Rohe A., Modelling fluidization and sedimentation using Material Point Method. *1st Pan-American Congress on Computational Mechanics - PANACM 2015. XI Argentine Congress on Computational Mechanics - MECOM 2015. S. Idelsohn, V. Sonzogni, A. Coutinho, M. Cruchaga, A. Lew & M. Cerrolaza (Eds)*, 2015.
[12] Martinelli M. *Soil-water interaction with Material Point Method. Double-Point Formulation*. Report on EU-FP7 research project MPM-Dredge PIAP-GA-2012-324522, 2016.
[13] Forchheimer, P. "Wasserbewegung durch Boden. *Z Ver Deutsch Ing* 45: 1782-1788, 1901.
[14] Bear J. *Dynamics of fluids in porous media*. New York: Elsevier, 1972.
[15] Ergun, S. Fluid flow through packed columns. *Chem. Engng Prog.*; 1952, 48, 89-94
[16] Plaxis2D – version 2016. www.plaxis.nl